Journal of Geodesy (2024) 98:109
https://doi.org/10.1007/s00190-024-01919-1

ORIGINAL ARTICLE

Flatness constraints in the estimation of GNSS satellite antenna phase center offsets and variations

Bingbing Duan[1] · Urs Hugentobler[1] · Oliver Montenbruck[2] · Peter Steigenberger[2] · Arturo Villiger[3]

Received: 14 August 2024 / Accepted: 6 November 2024

Abstract

Accurate information on satellite antenna phase center offsets (PCOs) and phase variations (PVs) is indispensable for high-precision geodetic applications. In the absence of consistent pre-flight calibrations, satellite antenna PCOs and PVs of global navigation satellite systems are commonly estimated based on observations from a global network, constraining the scale to a given reference frame. As part of this estimation, flatness and zero-mean conditions need to be applied to unambiguously separate PCOs, PVs, and constant phase ambiguities. Within this study, we analytically investigate the impact of different boresight-angle-dependent weighting functions for PV minimization, and we compare antenna models generated with different observation-based weighting schemes with those based on uniform weighting. For the case of the GPS IIR/-M and III satellites, systematic differences of 10 mm in the PVs and 65 cm in the corresponding PCOs are identified. In addition, new antenna models for the different blocks of BeiDou-3 satellites in medium Earth orbit are derived using different processing schemes. As a drawback of traditional approaches estimating PCOs and PVs consecutively in distinct steps, it is shown that different, albeit self-consistent, PCO/PV pairs may result depending on whether PCOs or PVs are estimated first. This apparent discrepancy can be attributed to potentially inconsistent weighting functions in the individual processing steps. Use of a single-step process is therefore proposed, in which a dedicated constraint for PCO-PV separation is applied in the solution of the normal equations. Finally, the impact of neglecting phase patterns in precise point positioning applications is investigated. In addition to an overall increase of the position scatter, the occurrence of systematic height biases is illustrated. While observation-based weighting in the pattern estimation can help to avoid such biases, the possible benefit depends critically on the specific elevation-dependent weighting applied in the user's positioning model. As such, the practical advantage of such antenna models would remain limited, and uniform weighting is recommended as a lean and transparent approach for the pattern estimation of satellite antenna models from observations.

Keywords GNSS · Phase center offsets · Phase variations · Flatness constraint · One-step processing · BeiDou-3 MEO antenna model

1 Introduction

Dynamic orbits of global navigation satellite system (GNSS) satellites are determined with respect to the center of mass (CoM), which is well defined by the laws of celestial mechanics (Hugentobler and Montenbruck 2017). GNSS measurements of various frequencies, however, refer to different phase centers of the transmitting antenna, which are

✉ Bingbing Duan
bingbing.duan@tum.de

Urs Hugentobler
urs.hugentobler@tum.de

Oliver Montenbruck
oliver.montenbruck@dlr.de

Peter Steigenberger
peter.steigenberger@dlr.de

Arturo Villiger
arturo.villiger@swisstopo.ch

[1] Institute for Astronomical and Physical Geodesy, Technical University of Munich, Arcisstr. 21, D-80333 Munich, Germany

[2] German Space Operations Center, Deutsches Zentrum für Luft- und Raumfahrt, Münchener Str. 20, D-82234 Weßling, Germany

[3] Federal Office of Topography (swisstopo), Seftigenstr. 264, CH-3084 Wabern, Switzerland

Published online: 27 November 2024

neither physical points nor unambiguously defined (Mader 1999). The total phase center correction to the geometric distance between satellite and receiver is therefore partitioned into a phase center offset (PCO) contribution and the supplementary phase variations (PV). Here, the satellite PCO is defined as the vector from the CoM to the mean antenna phase center, while the satellite PVs describe the deviation of the wavefront from a sphere around the mean phase center as a function of boresight angle and azimuth (Schmid and Rothacher 2003; Schmid et al. 2005).

As a one-way measurement system, GNSS could not contribute to determining the scale of the terrestrial reference frame (TRF), when manufacturer calibrations of satellite antenna PCOs were not available (Altamimi et al. 2002). Instead, PCOs and PVs of GNSS satellite antennas had to be estimated from observations of a global network aligning the TRF scale to that derived from Satellite Laser Ranging (SLR) and Very Long Baseline Interferometry (VLBI) techniques (Altamimi et al. 2002; Schmid et al. 2007, 2016). A number of studies discussed the relation between changes in satellite PCOs and the corresponding impact on TRF scale, station coordinates and tropospheric zenith delays (Springer TA 2000; Zhu et al. 2003; Ge et al. 2005; Cardellach et al. 2007; Rebischung 2014; Bruni 2016; Steigenberger et al. 2016). Recently, Montenbruck et al. (2022) did a comprehensive semi-analytical analysis on the relation of the TRF scale and GNSS PCOs in the Z-direction (Z-PCOs, which is perpendicular to the antenna panel plane and points nominally toward the center of the Earth). The impact-ratio values are about −0.051, −0.055, −0.041 and −0.046 for GPS, GLONASS, Galileo and BeiDou-3 satellites, respectively, but vary slightly with observation weighting strategies and elevation masks. Overall, a 10 cm change in the satellite's Z-PCO causes a change in station heights of about 5 mm or, equivalently, a 0.8 ppb scale change.

Recognizing the benefit of pre-flight antenna calibrations for geodetic applications, manufacturer calibrations for the PCOs of Galileo (GSC 2022), BeiDou (CSNO 2019b), GPS III (Lockheed Martin 2023) and QZSS satellites (Cabinet Office 2022) were publicly released. Steigenberger and Montenbruck (2023) and Duan et al. (2023) compared the estimated Galileo satellite PCOs to the calibrated values. X-PCOs show a bias of about 1 cm, while Y-PCOs are free of such bias. The ITRF2020-aligned Z-PCO estimates exhibit a systematic offset of −11 to −15 cm from the manufacturer calibrations reflecting a 0.7–1.0 ppb scale inconsistency. Consistency of Z-PCOs between various frequencies of Galileo satellites is better than 4 cm. In a related effort, Steigenberger et al. (2024) evaluated the pre-flight calibrations of GPS III satellites provided by the manufacturer Lockheed Martin. The estimated horizontal PCOs agree on a few-centimeters level and the ITRF2020-aligned Z-PCOs have a systematic bias of about 10 cm indicating a similar scale inconsistency as for the Galileo manufacturer calibrations. Matching results were also obtained for GPS IIF antenna calibrations discussed in Montenbruck et al. (2024), even though various unproven assumptions had to be made concerning the proper interpretation of the manufacturer data. For BeiDou-3, Xia et al. (2020), Zhao et al. (2022) and Zajdel et al. (2022) analyzed the consistency of manufacturer-calibrated PCOs for ionosphere-free linear combinations of different frequencies. The estimated Z-PCO values using B1I/B3I and B1C/B2a ionosphere-free linear combinations reveal an inconsistency of 10–20 cm.

With manufacturer calibrations for GNSS satellites and complementary chamber or robot calibrations of ground antennas (Zeimetz and Kuhlmann 2008; Wübbena et al. 2019; Kersten et al. 2022), the GNSS technique can, in principle, contribute to the determination of the TRF scale. However, Villiger et al. (2020) demonstrated a scale difference of about 1 ppb between the estimation from Galileo satellites and the scale of ITRF2014 (Rebischung and Schmid 2016). Similar work was also done by adding low earth orbiting (LEO) satellite measurements into global GNSS analyses (Haines et al. 2015; Glaser et al. 2020; Huang et al. 2021). In the realization of the most recent ITRF2020, a difference of 0.68 ppb + 0.018 ppb/a in the scale was observed between estimations from GNSS and SLR/VLBI by IGN (Altamimi et al. 2023; Rebischung et al. 2024). As a consequence, the GNSS technique was excluded from the determination of ITRF2020 scale. Same as before (Ray et al. 2013; Dilssner et al. 2010; Dach et al. 2011; Villiger et al. 2021), GNSS satellite-specific PCOs have to be repeatedly estimated by the International GNSS Service (IGS, Johnston et al. 2017) based on the scale of the latest ITRF version. The TRF solution from Deutsches Geodätisches Forschungsinstitut (DGFI), the DTRF2020, on the other side sees an agreement between VLBI and GNSS and uses these two techniques to define the scale (Blossfeld et al. 2022; Seitz et al. 2023a, b).

The phase center corrections are commonly separated into a constant part, the PCO and a directional varying part, the PVs. The separation into PCO and PVs leads to a parameterization that needs to be addressed. Typically, due to high correlations, satellite PCOs and PVs are estimated sequentially in two or more distinct steps including a possible normalization of the pattern based on user-defined minimization criteria. While it is generally assumed that the final results are independent of the order of the individual processing steps, a systematic comparison of antenna models obtained by first estimating PCOs and then PVs, with those obtained by first estimating PVs, then PCOs, is presently lacking. In particular, different weighting conditions of constraints for obtaining zero-mean and flat patterns will result in different satellite PCO and PV estimations. A combination of satellite PCOs/PVs determined from different methods therefore needs to be aligned to the same datum.

With this background, this contribution explains different minimization constraints mathematically and presents a lean and generic method to estimate antenna PCOs and PVs simultaneously in one processing step. The fundamental concepts and methodology are described in Sect. 2. Satellite PCO and PV results computed from different multi- and single-step methods are discussed in Sect. 3 for the sample case of the BeiDou-3 constellation. Assessments of different PVs in precise point positioning (PPP) are shown in Sect. 4. Finally, a summary and conclusions are presented based on the discussed results.

2 Methodology

As satellite antenna PCOs and TRF scale are strongly correlated, the estimation of satellite PCOs and PVs is only possible when the scale and robot- or chamber-based calibrations of ground antennas are available. In the following descriptions, we assume that both conditions are satisfied. Satellite PCOs and PVs have to be estimated together with satellite orbits and other parameters. As part of the observation model for carrier phase observations (Hauschild 2017), the antenna-related correction $\xi_{\mathrm{PCO/PV}}$ to the geometric distance between satellite and receiver is expressed as

$$\xi_{\mathrm{PCO/PV}} = -\boldsymbol{e}^T \cdot \boldsymbol{r}_{\mathrm{PCO}} + \xi_{\mathrm{PV}} \tag{1}$$

(Maqsood et al. 2017). Here, $\boldsymbol{e}$ denotes the satellite-to-receiver unit vector, $\boldsymbol{r}_{\mathrm{PCO}}$ is the PCO vector of the satellite defined in the satellite-body-fixed XYZ reference frame (Montenbruck et al. 2015), and ξ_{PV} represents the corresponding direction-dependent phase variations.

It can be recognized that Eq. (1) does not provide a unique distinction between satellite PCOs and PVs, as a change of $\Delta\boldsymbol{r}_{\mathrm{PCO}} = \widehat{\boldsymbol{r}}_{\mathrm{PCO}} - \boldsymbol{r}_{\mathrm{PCO}}$ from the total PCO $\widehat{\boldsymbol{r}}_{\mathrm{PCO}}$ can always be compensated by a corresponding change

$$\Delta\xi_{\mathrm{PV}} = \widehat{\xi}_{\mathrm{PV}} - \xi_{\mathrm{PV}} = +\boldsymbol{e}^T \cdot \Delta\boldsymbol{r}_{\mathrm{PCO}} \tag{2}$$

without affecting the total phase pattern correction $\xi_{\mathrm{PCO/PV}}$. Here, $\widehat{\xi}_{\mathrm{PV}}$ denotes the minimized satellite PVs that are free of satellite PCO contributions. An additional condition, e.g., a flatness constraint, for the PV patterns is therefore required, when estimating PCOs and PVs from observations to separate both effects in an unambiguous manner.

Furthermore, it is noted that ξ_{PV} is also ambiguous with respect to additive constants Δb that are indistinguishable from the carrier phase ambiguities and phase biases (Montenbruck et al. 2024). To deal with this issue, an additional condition, e.g., a zero-mean constraint for the satellite PVs, has to be applied to compute PCOs and PVs.

In this work for GNSS satellites, transmit antenna patterns are assumed to be rotationally symmetric about the boresight axis and can thus be described as a function of the boresight angle θ. Consistent with this, only the Z-component of $\Delta\boldsymbol{r}_{\mathrm{PCO}}$ (ΔZ_{PCO}) needs to be considered in the minimization of the phase patterns. Altogether, the phase pattern contribution ξ_{PV} to the observation model (1) can thus be expressed as

$$\xi_{\mathrm{PV}}(\theta) = -\cos(\theta) \cdot \Delta Z_{\mathrm{PCO}} + \Delta b + \widehat{\xi}_{\mathrm{PV}}(\theta) \tag{3}$$

where $\widehat{\xi}_{\mathrm{PV}}$ denotes zero-mean and flat satellite PVs over a certain θ angle range. Overall, Eqs. (1) and (3) provide the generic model for estimating the antenna phase center

$$\widehat{\boldsymbol{r}}_{\mathrm{PCO}} = \boldsymbol{r}_{\mathrm{PCO}} + (0, 0, \Delta Z_{\mathrm{PCO}})^T \tag{4}$$

and the minimized phase pattern $\widehat{\xi}_{\mathrm{PV}}(\theta)$ from GNSS observations along with suitable constraints for ΔZ_{PCO} and Δb.

2.1 Minimization conditions

Following Dach et al. (2015), a piecewise linear (polygonal) function $\xi_{\mathrm{PV}}(\theta)$ with $\xi_{\mathrm{PV}}(i\,\Delta\theta) = \xi_i$ for $i = 0, \ldots, n$ with a sampling interval $\Delta\theta = 1^\circ$ is applied in this work to describe the satellite PVs up to a maximum boresight angle $\theta_{\max} = n\Delta\theta$. In analogy with Eq. (3), a pattern vector $\boldsymbol{\xi} = (\xi_i)_{i=0,\ldots,n}$ may be transformed to a flat and zero-mean pattern $\widehat{\xi}_i$ by removing a PCO and bias contribution $(\Delta Z, \Delta b)^T$ based on minimization of the weighted square sum

$$\sum_{i=0}^{n} w_i \widehat{\xi}_i^2 \tag{5}$$

of the resulting grid points

$$\widehat{\xi}_i = \xi_i + \cos(\theta_i) \cdot \Delta Z_{\mathrm{PCO}} - \Delta b \; . \tag{6}$$

For given weights $\boldsymbol{w} = (w_i)_{i=0,\ldots,n}$, the least-squares solution for the PCO and bias contribution is given by

$$\begin{pmatrix} \Delta Z_{\mathrm{PCO}} \\ \Delta b \end{pmatrix} = (\boldsymbol{B}^T \boldsymbol{P} \boldsymbol{B})^{-1} \boldsymbol{B}^T \boldsymbol{P} \boldsymbol{\xi} \; , \tag{7}$$

where

$$\boldsymbol{B} = \begin{pmatrix} -\cos(\theta_0) & 1 \\ \vdots & \vdots \\ -\cos(\theta_n) & 1 \end{pmatrix} \tag{8}$$

denotes the design matrix and where $\boldsymbol{P} = \mathrm{diag}(\boldsymbol{w})$ is a diagonal weighting matrix.

For a given pattern vector $\boldsymbol{\xi}$, Eq. (7) can be used to find the PCO correction needed to obtain a flat and zero-mean-aligned phase pattern. Likewise, the relation can be used to constrain an estimated pattern $\widehat{\boldsymbol{\xi}}$ in the global adjustment of PCOs, patterns and other parameters from processing observations of a global network. In the latter case, a condition

$$\begin{pmatrix} 0 \\ 0 \end{pmatrix} \stackrel{!}{=} (\boldsymbol{B}^T \boldsymbol{P} \boldsymbol{B})^{-1} \boldsymbol{B}^T \boldsymbol{P} \widehat{\boldsymbol{\xi}} \tag{9}$$

is incorporated into the overall normal equations in the form of either a hard or soft constraint.

Depending on the specific application, different weighting schemes may be use in practice, out of which we highlight three basic concepts:

- *Case A:* In the most simple case, all grid points receive an equal (unit) weight $w_i = 1$. This approach enables a seamless application to 2-dimensional patterns (varying with azimuth A and off-boresight angle θ) and 1-dimensional (θ-dependent) patterns. Because of its simplicity and computational convenience, uniform weighting on an equidistant (A, θ) grid is widely applied in chamber calibrations of GNSS receive antennas (Kunysz 2010) as well as transmit antennas. Uniform weighting has, e.g., been applied in the 2-dimensional manufacturer calibrations of GPS satellite antennas (Montenbruck et al. 2024) and is traditionally used within the IGS to derive flat and zero-mean 1-D patterns for its antenna models.
- *Case B:* Conceptual concern with uniform weighting on an equidistant (A, θ) or θ grid stems from the fact that it is far from isotropic and overweights the boresight direction in relation to the solid angle covered by adjacent grid points. To cope with this deficiency, the use of a triangular grid with a near-equal spacing of grid points on the unit sphere has therefore been proposed as an alternative and applied for estimating phase centers and patterns of GNSS satellites in Zehentner (2016) and Strasser et al. (2019). In the 1-dimensional case considered here, an isotropic weighting can be approximated by assigning weights of $w_i = \sin(\theta_i) \cdot \Delta\theta$ to the individual grid points that describe the fractional area on the unit hemisphere covered by each θ interval.
- *Case C:* While the isotropic weighting copes with the limitations of uniform weighting on an equidistant grid, it is not necessarily representative of the conditions met in the joint adjustment of satellite PCOs or patterns from GNSS observations along with other parameters such as GNSS orbits and clock offsets. Here, the effective weights associated with a specific boresight angle are determined by the fractional observation density $\nu(\theta)$, which describes the fraction $dN/N = \nu(\theta)d\theta$ of observations within an infinitesimal interval $d\theta$ around θ, as well as possible elevation-dependent observation weights.

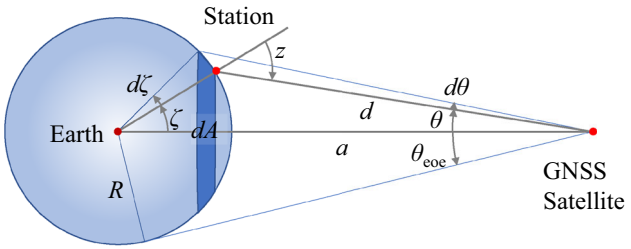

Fig. 1 Illustration of the region on the Earth's surface (dark blue) corresponding to observations within an interval $[\theta, \theta + d\theta]$ of boresight angles for a GNSS satellite at distance a from the center of Earth

To better understand the differences between observation-based weighting and the other alternatives, we evaluate the resulting effective weights for different GNSS constellations and observation weights. In a previous work, Montenbruck et al. (2022) has evaluated the observation density as a function of zenith angle at the receiving antenna based on a global network of 85 stations. Based on empirical evidence, the authors found a near-linear relation $\nu_z(z) \approx 0.8z$ that applies equally for GPS, GLONASS, Galileo and BeiDou satellites in medium Earth orbit (MEO) despite the slightly different altitudes. For the present work, we analytically compute the observation density as a function of the boresight angle, by considering the fractional amount of stations observing a satellite within the interval $[\theta, \theta + d\theta]$ under the assumption of a homogeneously distributed station network.

As illustrated in Fig. 1, the respective stations are located in a ring-shaped region of area dA on the Earth's surface with central angles in the range of ζ and $\zeta + d\zeta$. The fractional number of observations

$$\nu(\theta)d\theta = \frac{dA}{A} = \frac{2\pi R^2 \sin(\zeta) d\zeta}{4\pi R^2} \tag{10}$$

from this region then matches the ratio of dA and the total surface area A of the Earth. Based on the geometry of the station-Earth-satellite triangle, an infinitesimal change $d\theta$ of the boresight angle results in a change of

$$d\zeta = \frac{d}{R}\left(\frac{a}{R} \cdot \frac{a - d\cos\theta}{a\cos\theta - d} - \frac{d}{R}\right) d\theta \tag{11}$$

in the central angle, where a denotes the orbit radius, R is the Earth radius, and d is the satellite distance from the station. Upon combining Eqs. (10) and (11), the fractional observation density ν can be computed as a function of the boresight angle θ.

When processing GNSS observations for the adjustment of PCOs and patterns along with other parameters, a zenith-angle-dependent weighting function $\widehat{w}(z)$ is commonly

applied to account for the variation of measurement noise, multipath and atmospheric errors. The effective, boresight-angle-dependent weighting for the PCO/PV estimation is then given by the product $w(\theta) = \nu(\theta) \cdot \widehat{w}(z(\theta))$ of the relative observation density and the zenith-angle-dependent observation weight.

As discussed in Montenbruck et al. (2022), a variety of different weighting functions $\widehat{w}_i$ are presently used for carrier phase processing by individual IGS analysis centers. These include, for example,

$$\widehat{w}_1(z) = \cos^2(z) \tag{12}$$

$$\widehat{w}_2(z) = \begin{cases} 1 & \text{for } z < 60° \\ 4\cos^2(z) & \text{for } z > 60° \end{cases} \tag{13}$$

$$\widehat{w}_3(z) = \cos(z) \tag{14}$$

$$\widehat{w}_4(z) = (a + (1-a)\cos^2(z)) \text{ with } a = 0.15 \tag{15}$$

$$\widehat{w}_5(z) = \frac{a^2 + b^2}{a^2 + b^2/\cos^2(z)}, \text{ with } a = 5.5 \text{ and } b = 35 \tag{16}$$

Figure 2 shows the resulting weight function $w(\theta)$ for the example of the BeiDou-3 MEO constellation with an orbital radius of $a = 27900$ km and an edge-of-Earth boresight angle of about $\theta_{\text{eoe}} = 13.2°$. Irrespective of the zenith-angle weighting $\widehat{w}$, all weighting functions show a similar, quasi-linear increase with θ up to boresight angles of about 8°, but notable differences may be recognized closer to the edge of Earth. Considering only the observation density, i.e., $\widehat{w} = 1$, a steep increase of $w(\theta)$ with a pole at θ_{eoe} is encountered. For most other choices of $\widehat{w}$, the total weight remains bounded and decreases to zero at θ_{eoe}. As a result, peak weights are obtained in a region of boresight angles between about 9° to 12°. Obviously, PCO corrections and patterns obtained with such weighting functions will be notably different from those obtained with a uniform weighting as discussed above for Case A.

Complementary to the analytically computed weight functions, Fig. 2 also shows the effective weights $\widehat{w}_{1,\text{est}}(z)$ derived from the diagonal elements of the information matrix (normal equation) in the estimation of BeiDou-3 MEO patterns from a global network of 130 stations with a $\cos^2(z)$ weighting (see Sect. 3). The good agreement of $\widehat{w}_{1,\text{est}}(z)$ and $\widehat{w}_1$ confirms the validity of the analytical weighting model for a reasonably homogeneous station distribution and enables predictions of AC specific processing strategies on the estimated PCOs and patterns.

By way of example, Fig. 3 illustrates the impact of different weighting strategies on the phase pattern of the GPS III satellites, which closely matches that of the Block IIR-B and IIR-M satellites (Montenbruck et al. 2024) and is thus representative of a major fraction of the current GPS constellation. The individual results are based on the minimization of block-average GPS III patterns from the igs20.atx antenna

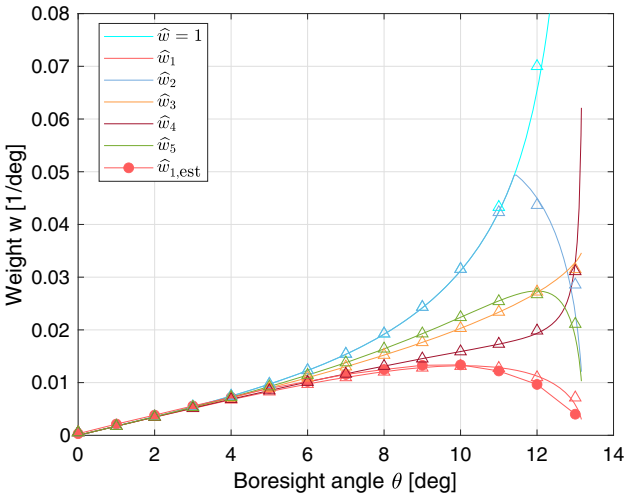

Fig. 2 Observation-dependent weighting $w = \nu \cdot \widehat{w}$ as a function of boresight angle computed for different zenith-angle-dependent observation weightings $\widehat{w}(z)$. $\widehat{w}_{1,\text{est}}(z)$ denotes the estimated weights from real data. The triangular symbols consider the weighting according to the piecewise linear representation of the PV

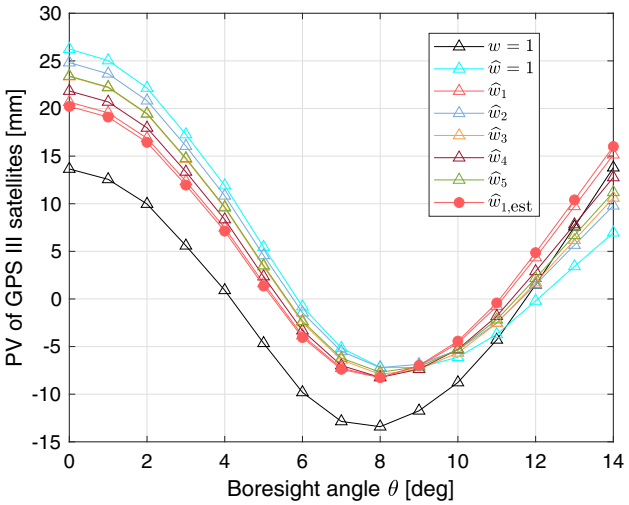

Fig. 3 GPS III satellite PVs minimized by using unit weighting ($w = 1$; black curve) and observation-dependent weighting ($w = \nu \cdot \widehat{w}$; colored curves) based on different $\widehat{w}(z)$

model on a 1° boresight angle grid up to a limiting angle of $\theta = 14°$ using Eq. (7). Significant differences may be noted between the unit weighting (Case A; $w = 1$, black curve) and the observation-dependent weightings (Case C; colored curves) for various choices of $\widehat{w}(z)$. All observation-based weight functions downweight contributions at small and large boresight angles and minimize the pattern amplitude in intermediate regions. This results in a systematic shift of about 5 mm between the two groups (black and colored curves) as well as differences of up to 20 mm in the variation from the center to the edge of the antenna field of view. Along with this, differences of about 65 cm in the corresponding Z-

Table 1 GPS III satellite Z-PCOs corresponding to different sets of minimized PVs from Fig. 3

Number	Weighting	Z-PCO difference
1	$w = 1$	0.0
2	$\widehat{w} = 1$	−65.4
3	$\widehat{w}_1$	−19.1
4	$\widehat{w}_2$	−51.1
5	$\widehat{w}_3$	−43.4
6	$\widehat{w}_4$	−31.0
7	$\widehat{w}_5$	−41.6

All values are given in [cm] relative to the PCOs obtained with uniform weighting

PCO estimates are found. GPS III satellite Z-PCO biases corresponding to different sets of minimized PVs are shown in Table 1.

2.2 Estimating satellite PCOs and PVs from observations

Within the IGS, a multi-step approach is commonly used to determine GNSS satellite PCOs and PVs from observations of a global receiver network. In each step, either PCOs or PVs are estimated to account for the correlation of these parameters, which inhibits a joint estimation in an unconstrained adjustment process:

- In a first step, an a priori phase pattern is adopted, based on which the unknown PCOs can be adjusted along with satellite orbits, clocks and other parameters. Receiver antenna patterns are assumed to be known from independent calibrations, and station coordinates are constrained to a given TRF to mitigate a singularity that would arise in the joint adjustment of satellite PCOs and station heights. In the absence of other information, a zero pattern may be assumed for the transmit antennas (Steigenberger et al. 2016; Xia et al. 2020; Zajdel et al. 2022). Alternatively, an approximate pattern from other sources, e.g., a past IGS calibration or a manufacturer calibration, can be employed (Schmid et al. 2007; Dilssner et al. 2010; Steigenberger and Montenbruck 2023). The PCOs obtained in this way minimize the weighted square-sum of the carrier phase residuals taking into account the actual distribution of observations with boresight angle and the zenith-angle-dependent weight function.
- Next, an improved pattern can be obtained from either the carrier phase residuals and the a priori pattern of the previous step or an independent least-squares adjustment of the pattern parameters while keeping the PCOs fixed to the previously determined values (Schmid and Rothacher 2003; Schmid et al. 2007). Overall, this yields fully consistent pairs of PCOs and PVs for the individual satellites that offer an accurate modeling of the respective carrier phase observations. By their design, the resulting patterns are minimized subjecting to weighting with the observation density and the zenith-angle-dependent weight function $\widehat{w}(z)$ of the adjustment process as outlined above in the discussion of Case C.
- Patterns and PCOs constructed in this way by different analysis centers (ACs) will naturally deviate from each other due to the implicit use of different weight functions, even though each PCO-PV pair will ideally provide the same range correction. For enabling a combination of patterns from individual ACs, a re-normalization of the individual AC patterns needs to be performed using a common convention for the pattern minimization and a subsequent correction of the associated PCOs. In view of its simplicity and transparency, the uniform weighting on an equidistant grid (Case A) is most widely used for this purpose (Schmid and Rothacher 2003; Dilssner et al. 2010). The transformation changes the individual PCO and PV values for a given AC, but retains the total range correction. Re-normalized PVs from different ACs may be used to compute AC-mean patterns from, e.g., a simple arithmetic mean of all contributing centers.
- If desired, e.g., in the context of IGS reference frame updates, PCOs may be re-adjusted with the mean patterns from the previous step and AC-mean PCOs can be obtained for a fully consistent conventional antenna model.

To avoid the complexity and iterative nature of the multi-step method, a lean and generic single-step method is presented here, which allows to estimate satellite PCOs and PVs simultaneously in a combined adjustment process. The idea is to adopt zero-mean and flatness conditions as additional constraints and jointly use them with the GNSS carrier phase observation equations in the overall parameter adjustment. Mathematically, the constraints are defined by Eq. (9) and can be incorporated into the normal equations as either a hard constraint by eliminating two independent parameters or as a "soft" constraint in the form of a pseudo-observation with "infinite" weight.

By applying the constraint conditions, PCOs and PVs can be concurrently estimated without causing a singularity. Depending on the specific choice of weights w_i for the individual grid points ξ_i of the antenna pattern, different minimization criteria maybe implemented in accord with application-specific needs. Most importantly, this includes an observation-based weighting to obtain PCO/PV pairs designed for minimizing carrier phase residuals when considering only the PCO (consistent with Case C), or the common uniform weighting of all boresight angle grid points (consistent with Case A).

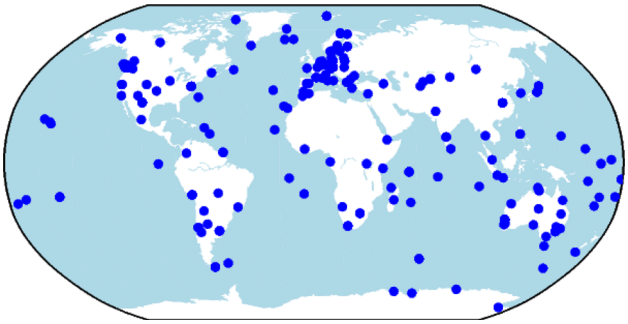

Fig. 4 Ground network for BeiDou-3 antenna model generation

Mathematically, the single-step estimation with flatness and zero-mean constraint is fully equivalent to the multi-step approach under the provision that identical weighting concepts are applied in both approaches for separating PCO and PV contributions to the modeled carrier phase range. However, the single-step approach enables a direct estimation of both PCOs and PVs in a single least-squares estimation process and enables a transparent and unambiguous interpretation of the resulting patterns at the moderate expense of adding the zero-mean and flatness constraints to the normal equations. To further illustrate the equivalence of both approaches in a practical use case, the estimation of BeiDou-3 MEO antenna patterns is discussed in Sect. 3.

3 BeiDou-3 antenna model estimation

To compare the generation of an observation-based GNSS antenna model using different strategies for PCO and PV estimation, BeiDou-3 is selected as an example for our study. Other than GPS, GLONASS and Galileo, the Chinese BeiDou-3 system (Yang et al. 2018) is currently the only global navigation satellite system, which lacks a comprehensive set of antenna data consistent with the IGS20 reference frame (Altamimi et al. 2023) as part of the igs20.atx antenna model (Villiger 2022). Even though frequency-specific PCO values have previously been released for all BDS-3 satellites, details of these calibrations are not publicly documented and the corresponding phase variations have not been disclosed so far. Furthermore, previous studies by Zajdel et al. (2022), Xia et al. (2020), Yuan et al. (2024), and Huang et al. (2023) have raised serious concerns about the self-consistency of factory calibrations for the MEO satellites built by one of the two manufacturers.

Due to the lack of consolidated models and metadata as well as the limited time span from the full-constellation service to the ending epoch of the IGS repro3 campaign that served as the basis for establishing the GNSS contribution to the ITRF2020 (Rebischung et al. 2024), BeiDou-3 could not be considered for the generation of the IGS20 reference frame and the igs20.atx antenna model. While the use of unmodified BDS-3 manufacturer calibrations in igs20.atx represents a compromise for enabling multi-GNSS processing, it is known to cause inconsistencies in precise point positioning with other GNSSs and to be incompatible with the IGS20 scale.

In view of these limitations, BeiDou-3 still requires generation of a consistent, observation-based antenna model within the IGS. It is therefore ideally suited to illustrate the practical application of different processing strategies and weighting concepts in the estimation of PCOs and PVs from scratch.

3.1 Observations and processing standards

For the BeiDou-3 processing, a subset of about 130 ground tracking stations from the IGS network is used (Fig. 4). Aside from a reasonably homogeneous global distribution, stations have been selected based on the availability of dedicated receiver antenna calibrations in all processed frequency bands as part of the igs20.atx antenna model. The processing interval covers a one-year period from day 001 to day 365 of year 2023, which aims to minimize the impact of seasonal and draconitic errors in the estimated antenna parameters. In view of their improved noise and multipath performance, the modernized B1C/B2a signals of the BeiDou-3 satellites (Lu et al. 2019) are used instead of the legacy B1I/B3I signals.

A summary of observation data and processing settings is given in Table 2. For the GNSS orbit modeling, the ECOM2 solar radiation pressure model (Arnold et al. 2015) excluding the 4th-order terms in the satellite–Sun direction is employed. Earth radiation and antenna thrust effects are modeled (Rodriguez-Solano et al. 2012; Steigenberger et al. 2018).

For the antenna pattern estimation, GPS, Galileo and BeiDou-3 observations are jointly processed in daily arcs. A double-difference processing is employed that eliminates clock and inter-system bias parameters. Aside from the satellite orbits and solar radiation pressure parameters, the station coordinates, tropospheric zenith delays and gradients, earth rotation parameters and geocenter coordinates are estimated in a global parameter adjustment. No-net-rotation, no-net-translation and no-net scale conditions are applied for verified IGS20 datum stations. The final satellite PCOs/PVs are estimated by stacking daily normal equations over 365 days for satellite-specific PCOs and block-specific PVs.

3.2 BeiDou-3 antenna characteristics

The global MEO constellation of the BeiDou-3 system is presently made up of three different types of satellites built by two different manufacturers, namely the China Academy of Space Technology, CAST, and the Shanghai Engineer-

Table 2 Processing settings

Settings	Value
Software	Bernese GNSS Software 5.5, modified (Dach et al. 2015)
Network	130 stations
Observations	GPS: C1W, C2W, L1W, L2W
	Galileo: C1C, C1X, C5Q, C5X, L1C, L1X, L5Q, L5X
	BeiDou-3: C1P, C1X, C5P, C5X, L1P, L1X, L5P, L5X
	Double-differenced ionosphere-free
Data sampling	150 sec
Data interval	24 h
Elevation cutoff	5 deg
Elevation-dependent weighting	$\widehat{w} = \cos^2(z)$
Troposphere model and mapping function	VMF3 (Landskron and Böhm 2018)
Receiver antenna model	igs20.atx (Villiger 2022)
Satellite antenna model	igs20.atx (Villiger 2022); a priori for GPS, Galileo, BeiDou-3
Solid earth and ocean tides	IERS 2010 (Petit and Luzum 2010)
Phase wind-up	Modeled (Wu et al. 1993)
Ocean loading	FES2014b (Lyard et al. 2021)
Orbit modeling	
Solar radiation pressure (SRP)	7-parameter ECOM2 (Arnold et al. 2015)
Earth radiation	Applied (Rodriguez-Solano et al. 2012)
Antenna thrust	Applied (Steigenberger et al. 2018)
Parameters	
Orbits	24 h, six Keplerian elements plus seven ECOM2 parameters
Satellite antenna model	PCO (X,Y,Z) and PV (1-deg grid)
Station coordinates	24 h, no-net-rotation, no-net-translation, no-net-scale
	with respect to IGS20
Earth rotation parameters	24 h, piecewise linear
Geocenter coordinates	24 h
Tropospheric zenith delay	2 h, piecewise linear
Tropospheric gradients	24 h
Ambiguities	Fixed to integers
	SIGMA method (Dach et al. 2015)

ing Center for Microsatellites, SECM. In view of different metadata that suggests a slightly modified platform design (CSNO 2019a, c), two subtypes of SECM satellites known as SECM-A and SECM-B are distinguished within the IGS. Even though this distinction does not necessarily imply use of a different antenna design, we prefer to consider three independent groups of satellites and antenna patterns (CAST, SECM-A and SECM-B) for the BeiDou-3 transmit antenna model. As will be shown shortly, this decision is well justified by small, but well discernible differences between the estimated SECM-A and -B patterns.

For an initial characterization of the BeiDou-3 antennas, the well-established multi-step method is used to estimate a consistent set of PCOs and PVs of the three antenna types. In a first step, block-specific PVs are estimated while fixing the PCOs to the manufacturer calibrations in igs20.atx. Given the scale inconsistency between the manufacturer data and the IGS20 reference frame, the resulting raw patterns are dominated by uncompensated phase center contributions. Normalized pattern are therefore computed by removing these contributions based on Eq. (7) with equal weights for each point of the boresight angle grid. As a third and final step, the satellite-specific PCOs are corrected to account for the contribution of the newly estimated, minimized phase patterns.

The maximum boresight angle for BeiDou-3 MEO satellites amounts to 13.2°, when considering an elevation cutoff angle of 0°. For this reason, we confine ourselves to an equidistant 1° grid up to $\theta_n = 13°$. Phase variations beyond this limit would still be required for processing of low-

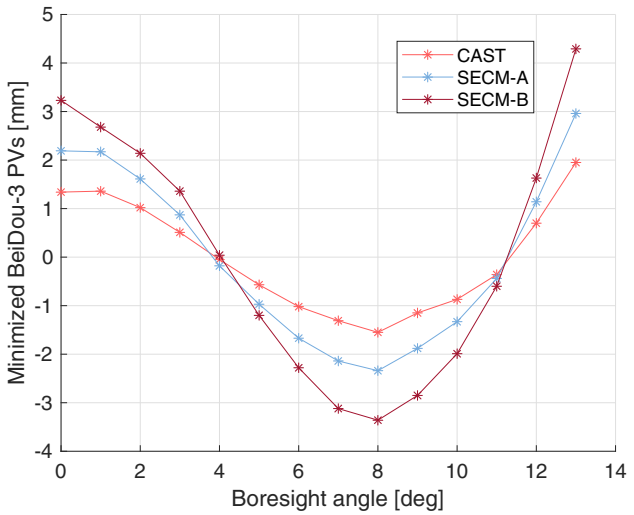

Fig. 5 Boresight-angle-dependent phase patterns of the three types of BeiDou-3 MEO satellites. All patterns are minimized using uniform weighting over the 1° grid

elevation observations, but can best be obtained by linear extrapolation from the last grid points or by including measurements from satellites in low Earth orbit (LEO) into the solution (Qu et al. 2024).

Figure 5 shows the minimized block-specific phase pattern of the three types of BeiDou-3 MEO satellites. The phase variations show an overall similarity with those of the GPS III satellites (Fig. 3) but are notably smaller in amplitude. Depending on the specific satellite type, the normalized patterns are confined to a range of roughly ±2 to ±4 mm. It is also worth noting that the PVs of the SECM-B satellites show a roughly 50% (or 1 mm) higher amplitude than those of the SECM-A satellites. This confirms the suspicion of a slightly modified satellite environment or even antenna design.

The differences of the estimated and manufacturer-calibrated BeiDou-3 satellite PCOs are plotted in Fig. 6. Agreements of the horizontal PCOs are in most cases better than 2 cm. Consistency for the Y-PCOs is clearly better than that for the X-PCOs. A similar performance has also been observed by Steigenberger and Montenbruck (2023) and Steigenberger et al. (2024) for Galileo and GPS III satellites, where it could be attributed to the deficiencies of the solar radiation pressure modeling.

In contrast to the horizontal PCOs, the Z-PCO estimates show both large positive and negative differences compared to the manufacturer calibrations, which is not only caused by the scale inconsistency. CAST MEO satellites show both positive and negative differences ranging from −10–25 cm compared to manufacturer calibrations, and a similar performance is also observed for SECM-A satellites. Z-PCO estimations for the two SECM-B satellites show a negative difference of about −25 cm compared to the corresponding calibrations. These results are in good overall agreement with earlier findings of Zajdel et al. (2022), Xia et al. (2020), Yuan et al. (2024) and Huang et al. (2023), when taking into account systematic differences of the underlying reference frames.

Even though the proper interpretation of the BeiDou-3 manufacturer PCO calibration remains unclear due to lacking information on the associated phase variations and their minimization condition, an unexpectedly large scatter of PCO differences can also be observed in Fig. 6 within groups of satellites presumably using the same antenna type. In view of the pronounced inconsistencies between estimated and manufacturer-calibrated PCOs, the use of an observation-based antenna model is therefore deemed mandatory for precise geodetic applications until further documentation of the factory calibrations becomes available, and increased confidence in their quality and proper usage can be gained.

3.3 Differences between different multi-step and one-step solutions

For further discussion of different approaches to the estimation of phase center offsets and variations, we compare the results obtained for BeiDou-3 CAST satellites in two alternative multi-step scenarios with those of the single-step estimation (Table 3). In the latter case, two different weighting functions are used as constraints, and it is demonstrated that the single- and multi-step methods yield consistent results under the provision of matching weighting concepts.

We confine the comparison to the group of CAST satellites, which currently constitutes the majority of satellites in the global BeiDou-3 constellation. Even though the amplitude of phase variations is smaller for this group than for the SECM-A and SECM-B satellites, the pattern shape is sufficiently similar to make the results applicable for the entire constellation. Building up on the basic methodology introduced in Sect. 2.2, a total of four different scenarios is tested:

- *Scenario-1:* Here, block-specific satellite phase patterns $\boldsymbol{\xi} = (\xi_i)_{i=0,\ldots,13}$ at the 1° grid points are computed in a first step with satellite PCOs fixed to manufacturer calibrations. As the sole constraint, a zero-mean condition based on unit weights $w(\theta_i) = 1$ is applied in this step for separating carrier phase ambiguities and constant phase pattern contributions b. In a second step, the estimated satellite PVs are minimized based on the same unit weighting $w(\theta_i) = 1$. The PCO corrections ΔZ estimated in this step for each satellite are finally used to update the a priori PCOs. The scenario essentially matches the approach used in Sect. 3.2 to derive the basic characteristics of the BeiDou-3 transmit antennas. It has similarly been used to obtain initial phase pattern estimates for complementing the manufacturer-

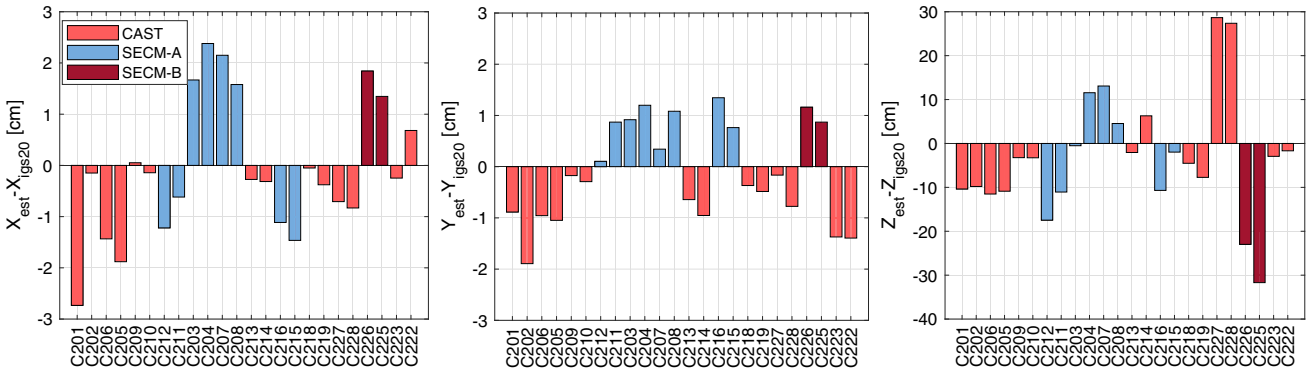

Fig. 6 Differences between estimations from Scenario-1 and manufacturer-calibrated PCOs of BeiDou-3 MEO satellites as given in the igs20.atx antenna model

Table 3 Description of different scenarios for single- and multi-step estimation of phase center offsets and patterns

Scenarios	Description	Weighting
Scenario-1	multi-step, PV-PCO	Unit weight $w = 1$ in zero-mean and flatness conditions
Scenario-2	multi-step, PCO-PV	Observation-dependent weight $w = \nu \cdot \widehat{w}_1$
Scenario-3	one-step, PV&PCO	Unit weight $w = 1$ in zero-mean and flatness constraint
Scenario-4	one-step, PV&PCO	Observation-dependent weight $w = \nu \cdot \widehat{w}_1$ in zero-mean and flatness constraint

calibrated PCOs of the GPS III satellites in the igs14.atx antenna model (Villiger 2019).

– *Scenario-2:* Rather than starting with the phase pattern estimation, satellite-specific PCOs are first adjusted in this approach without including any a priori phase pattern into the carrier phase modeling. The resulting phase center location minimizes the weighted root-sum-square phase residuals over the covered boresight angle range, which corresponds to an effective weighting $w(\theta) = \nu(\theta) \cdot \widehat{w}(\theta)$ of individual boresight angles. In a second step, block-specific satellite PVs are adjusted from observations while keeping the PCOs fixed to the values obtained in the first step. An additional zero-mean constraint is applied to separate constant phase pattern contributions from carrier phase ambiguities. This constraint must be based on the same observation-based weighting as used in the first step, to ensure full consistency of the combined set of PCOs and PVs. For the actual tests, a zenith-angle-dependent weight function $\widehat{w}_1(\theta) = \cos^2(\theta)$ has been adopted in the PCO and PV adjustment. Practical use cases of Scenario-2 include the PCO-only estimation of the early Galileo satellites (Steigenberger et al. 2016) and BDS-3 satellites (Zajdel et al. 2022).
– *Scenario-3:* Satellite PCOs and PVs are estimated in one step. A unit weight ($w_i = 1$) is used in the flatness and zero-mean constraint (Eq. (9)) to separate both parameters.

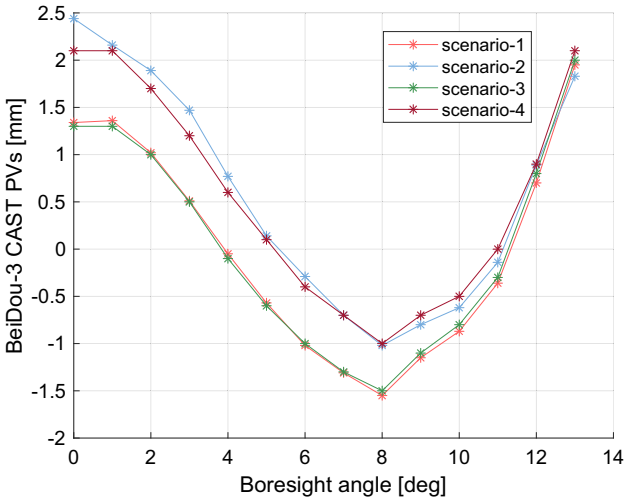

Fig. 7 Boresight-angle-dependent phase variation patterns estimated from different scenarios for BeiDou-3 CAST MEO satellites

– *Scenario-4:* Similar to Scenario-3, the satellite PCOs and PVs are estimated in a single step, but an observation-based weighting $w_i = \nu(\theta_i) \cdot \widehat{w}_1(\theta_i)$ is used in the constraint.

Figure 7 shows the block-mean PVs of the BeiDou-3 CAST MEO satellites obtained in the four scenarios, while the corresponding PCO estimates for each satellite are illustrated in Fig. 8. In accord with expectations, the results of single- and multi-step approaches closely match each other when using consistent weighting functions in the estimation

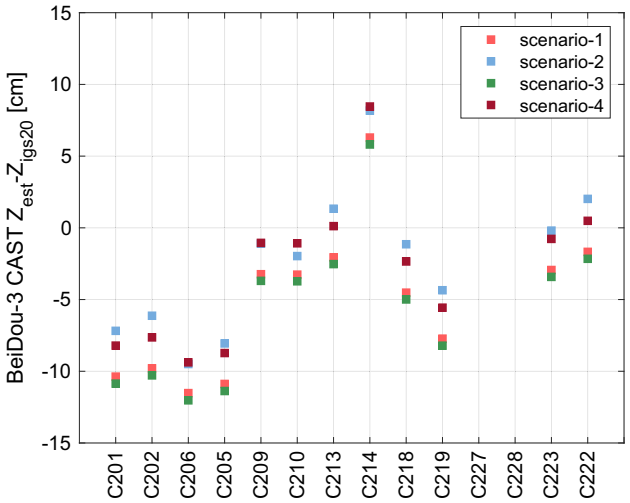

Fig. 8 Z-PCOs estimated from different scenarios for BeiDou-3 CAST MEO satellites

and constraint conditions. This is best seen for Scenario-1 and Scenario-3, which exhibit representative differences of less than 0.1 mm in the estimated patterns and at most 5 mm in the associated PCOs. Slightly larger differences of up to 0.3 mm and 1.5 mm show up in the comparison of Scenario-2 and Scenario-4 despite their conceptual similarity. These differences can be attributed to the fact that part of the unmodeled phase pattern in the PCO adjustment of Scenario-2 is absorbed in the estimated carrier phase ambiguities. This causes a slightly different PCO and residual pattern than in the joint PCO/PV estimation of Scenario-4.

The four tests once more illustrate the impact of different weighting on the estimated phase center locations and phase patterns. In view of the moderate overall amplitude of the BeiDou-3 antenna patterns, the respective changes are likewise at the level of about one millimeter (PVs) or a few centimeters (PCOs). Similar effects, albeit with a ten times higher amplitude would, however, be observed for GPS Block ÌIR-M or GPS III satellites with a similar pattern shape but notably larger variations.

Concerning the methodology for estimating PCOs and PVs from observations, different orders (PCO-PV vs. PV-PCO) may be considered in a multi-step approach. While the order itself does not have any direct impact on the results, it is often accompanied by different "natural" choices of the boresight-angle-dependent weighting. As such, different, but self-consistent PCO/PV pairs are typically obtained from the two approaches. In a single-step approach, PCOs and PVs are jointly estimated in a single last-squares adjustment. This offers full and transparent control over the weighting used in the constraint equation for the separation of the two constituents. Inconsistencies in the weighting, which may inadvertently occur in a multi-step approach for the weighting of the PCO and PV estimation steps, cannot occur in a single-step estimation, such ensuring full consistency in all cases.

4 Positioning

As analyzed in the previous sections, satellite antenna PCOs and PVs estimated from different methods may exhibit notable differences depending on the boresight-angle-dependent weighting in the zero-mean and the flatness conditions. Nevertheless, individual antenna models, i.e., pairs of PCOs and PVs generated with different weighting, provide consistent range corrections. As such, the specific weighting used to separate PCO and PV contributions in the overall range correction does not affect the positioning results for precise point positioning applications with and without ambiguity resolution (PPP, PPP-AR).

For the PPP/PPP-AR users, it is important to apply the same satellite antenna model (PCO and PV corrections) as that employed in the determination of satellite orbit, clock and, optionally, phase bias products. However, various real-time correction services, such as the Galileo High Accuracy Service (HAS; EU 2022; Fernandez-Hernandez et al. 2022) and the BeiDou-3 PPP-B2b service (CSNO 2020; Liu et al. 2020), employ a simplified observation model for their user algorithms, in which the orbit and clock corrections are jointly referred to a "phase center" of unspecified nature, while phase variations are ignored. In this section, we therefore evaluate the overall impact of satellite phase patterns on the positioning results.

As phase patterns for BeiDou-3 satellites are comparatively small, we take the GPS III satellites as an example, which closely match those of Block IIR-B/M satellites and were already addressed in Sect. 2.1. Minimized PVs for GPS III satellites based on different weighting strategies are shown in Fig. 3.

To assess the impact of neglected phase patterns in PPP solutions, we evaluate the differential changes in epoch-wise, least-squares precise point positioning solutions caused by the consideration of the phase variations in the modeled carrier range. A seven-day period (January 1-7, 2023) with GPS observations sampled at 900 s intervals is considered for this analysis. A 5° elevation mask is applied, and observations are weighted with an elevation-dependent function $\widehat{w}(z) = \cos^2(z)$. For simplicity and transparency, all active GPS satellites in the test period are assumed to use the same antenna type. Depending on their geographic location and their position relative to the GPS constellation, individual stations exhibit slightly different position errors when neglecting the transmit antenna phase patterns. For better diversity, we therefore include a total of five stations randomly distributed around the globe into the overall statistics.

Table 4 Mean ± standard deviation of epoch-wise station position errors caused by the neglect of phase variations in single point positioning solutions for GPS III antenna patterns

Number	Weighting	East	North	Up
1	$w = 1$	-0.2 ± 3.7	-1.4 ± 7.3	7.1 ± 14.4
2	$\widehat{w} = 1$	-0.3 ± 4.0	-1.4 ± 7.8	-18.5 ± 15.1
3	$\widehat{w}_1$	-0.2 ± 3.7	-1.4 ± 7.4	-0.3 ± 14.6
4	$\widehat{w}_2$	-0.3 ± 3.9	-1.4 ± 7.7	-12.9 ± 14.9
5	$\widehat{w}_3$	-0.3 ± 3.9	-1.4 ± 7.6	-9.9 ± 14.8
6	$\widehat{w}_4$	-0.3 ± 3.8	-1.4 ± 7.5	-5.0 ± 14.7
7	$\widehat{w}_5$	-0.3 ± 3.9	-1.4 ± 7.6	-9.2 ± 14.8

For each case, the weight function used in the flatness and zero-mean conditions for the pattern generation is specified. The corresponding phase patterns as a function of boresight angle are shown in Fig. 3. All values in [mm]

Table 4 shows mean and standard deviation of epoch-wise position errors caused by the neglect of individual phase patterns in PPP results affected by different satellite PVs for the full set of stations over the entire data arc. Overall, the root-mean-square (RMS) position errors roughly reflects the amplitude of the neglected phase variations. In the horizontal components, errors of 4–8 mm are encountered. A small nonzero-mean error is encountered, which reflects the fact that the impact of phase pattern errors on the individual station positions does not average out completely over the daily observation arcs.

In view of the inferior dilution of precision (Langley et al. 2017), the impact of neglected phase variations is most pronounced in the up-direction. While the standard deviations of the position errors amount to roughly 15 mm in all cases, notably differences may be observed for the systematic height bias. Depending on the specific weight function used in the pattern minimization, systematic height errors of up to roughly 2 cm are encountered. On the other hand, a near-zero height bias is obtained when considering a pattern minimized with the observation-based weighting $w = \nu \cdot \widehat{w}_1$ (third test case of Table 4). This is consistent with the earlier finding that observation-based weighting is equivalent to minimizing the residuals in a PCO-only modeling. In the specific case considered here, the weight function $\widehat{w}_1 = \cos^2(z)$ is likewise used for weighting observations in the positioning test as well as the generation of the respective phase pattern. Thanks to this consistency, no systematic station height offset shows up when neglecting the pattern.

However, notable height biases are still encountered when neglecting phase patterns, if the observation weighting in the positioning differs from that used in the pattern generation. Given the wide variety of elevation-based observation weight functions used in present PPP tools, it is therefore impossible to identify a "best" observation-based weighting scheme for the minimization of antenna patterns. In particular, an observation-based weighting in the pattern generation does not offer universally applicable advantages compared to, e.g., the uniform weighting (Case 1 of Table 4).

5 Summary and conclusion

The accurate modeling of carrier phase measurements in GNSS positioning and orbit determination applications depends on proper knowledge of the GNSS transmit antenna phase center location and the associated phase variations. Here, the phase center is considered as fictitious point relative to which the antenna wavefront is described by an approximate sphere, while the phase variations describe line-of-sight-dependent differences between the actual wavefront and the sphere around the assumed center. The partitioning of the entire range correction into a phase center offset and the associated phase variations is largely arbitrary, but commonly based on a minimization of the remaining phase variations. Depending on the specific flatness criterion, different PCO/PV pairs will be obtained, which yield identical overall range corrections, but result in different pattern shapes and amplitudes.

When estimating PCOs from observations of a global receiver network without prior knowledge of the phase patterns, an observation-based weighting is implicitly used, which depends on the actual number of observations in a given boresight angle range as well as the elevation-dependent weighting of carrier phase measurements in the parameter adjustment. The resulting PCOs and residual patterns may differ notably from PCOs and PVs based on a uniform weighting that is more commonly applied in manufacturer calibrations. An analytical model of an observation-based weighting function is derived and the impact of different weighting schemes in the minimization criterion is illustrated for the example of the GPS IIR-M/III antenna patterns. Here, differences of 10 mm and 65 cm, respectively, may be encountered in the resulting PVs and PCOs, when considering different boresight-angle-dependent weighting for the PCO/PV separation.

Use of a single-step PCO/PV estimation with explicit flatness and zero-mean constraints is suggested as an alternative to the traditional approach for generating GNSS transmit antenna models, in which PCOs and PVs are estimated in

separate steps while fixing one of the two parameter sets. The single-step approach enables a transparent application of a selected flatness condition and avoids the use of potentially inconsistent or alternating minimization criteria in the multi-step PCO/PV estimation. Differences between the various approaches are highlighted for the example of BeiDou-3 MEO antenna models that have been newly derived in this study to overcome known inconsistencies in the respective manufacturer PCO calibrations and the lack of corresponding phase patterns.

For precise point positioning applications, the use of antenna models based on observation-based weighting promises to minimize both carrier phase residuals and positioning errors in applications, which neglect the phase pattern contribution and consider only the phase center offset in the observation models. Examples of such applications include real-time correction services that directly provide orbit and clock information relative to the antenna phase center and do not involve explicit use of transmit antenna models in the positioning algorithms. Practical tests with GPS III antenna patterns show that use of antenna models based on observation weighting can indeed avoid a systematic height bias, when neglecting the respective phase variations in the position estimation. However, this benefit can only be materialized if the same elevation-dependent observation weighting is used in the pattern generation and the user positioning. In view of diverse weighting schemes applied in current PPP software packages, this condition can hardly be met in practice. In view of these limitations, use of antenna models based on uniform weighting over an equidistant grid of boresight angles in the pattern minimization is suggested as a lean and transparent option for a standardized representation of GNSS transmit antenna models.

Acknowledgements We would like to acknowledge the efforts of the station operators and data centers supporting IGS. Calculations are done using resources of the Leibniz Supercomputing Center (LRZ).

Author Contributions UH and BD proposed the general idea. BD, UH, OM and PS discussed the methodology, results and the structure of the manuscript. BD did the computation and prepared the draft manuscript. All authors analyzed the results and contributed individually to the writing of the manuscript.

Funding Open Access funding enabled and organized by Projekt DEAL.

Data availability GNSS data used are publicly available from the International GNSS Service (IGS) data centers, e.g., CDDIS: https://cddis.nasa.gov/archive/gnss/data/.

Code Availability Calculations are based on the Bernese GNSS Software (license available, University of Bern) and its specific modifications by the authors (not public).

Declarations

Conflict of interest Not applicable.

References

Altamimi Z, Sillard P, Boucher C (2002) ITRF2000: a new release of the international terrestrial reference frame for earth science applications. Solid Earth J Geophys Res. https://doi.org/10.1029/2001JB000561

Altamimi Z, Rebischung P, Collilieux X, Métivier L, Chanard K (2023) ITRF2020: an augmented reference frame refining the modeling of nonlinear station motions. J Geod. https://doi.org/10.1007/s00190-023-01738-w

Arnold D, Meindl M, Beutler G, Dach R, Schaer S, Lutz S, Prange L, Sośnica K, Mervart L, Jäggi A (2015) CODE's new solar radiation pressure model for GNSS orbit determination. J Geod 89(8):775–791. https://doi.org/10.1007/s00190-015-0814-4

Blossfeld M, Seitz M, Glomsda M, Angermann D, Rudenko S, Zeitlhöfler J (2022) DTRF2020: the ITRF 2020 realization of DGFI-TUM. In: AGU Fall Meeting Abstracts, G12A–04

Bruni S (2016) Combination of GNSS and SLR measurements: contribution to the realization of the terrestrial reference frame. Phd thesis, UniversitÃ di Bologna, https://doi.org/10.6092/UNIBO/AMSDOTTORATO/7636

Cabinet Office (2022) QZSS satellite information. Tech. rep., Government of Japan, National Space Policy Secretariat, https://qzss.go.jp/en/technical/qzssinfo/index.html

Cardellach E, Elósegui P, Davis J (2007) Global distortion of GPS networks associated with satellite antenna model errors. Solid Earth J Geophys Res. https://doi.org/10.1029/2006JB004675

CSNO (2019a) Definitions and descriptions of BDS/GNSS satellite parameters for high precision applications (in Chinese). Tech. Rep. BD 420025-2019, China Satellite Navigation Office, http://www.beidou.gov.cn/yw/gfgg/201911/W020191126317485269344.pdf

CSNO (2019b) Satellite antenna phase centers of BDS, China Satellite Navigation Office. http://en.beidou.gov.cn/SYSTEMS/Officialdocument/201912/P020200323536112807882.atx

CSNO (2019c) Satellite information of BDS, China Satellite Navigation Office. http://en.beidou.gov.cn/SYSTEMS/Officialdocument/201912/P020200323536298695483.zip

CSNO (2020) BeiDou Navigation Satellite System Signal In Space Interface Control Document Precise Point Positioning Service Signal PPP-B2b, Version 1.0, China Satel-

lite Navigation Office. http://www.beidou.gov.cn/xt/gfxz/202008/P020200803362062482940.pdf
Dach R, Schmid R, Schmitz M, Thaller D, Schaer S, Lutz S, Steigenberger P, Wübbena G, Beutler G (2011) Improved antenna phase center models for GLONASS. GPS Solut 15(1):49–65. https://doi.org/10.1007/s10291-010-0169-5
Dach R, Lutz S, Walser P, Fridez P (2015) Bernese GNSS Software version 5.2. User manual, Astronomical Institute. Bern: University of Bern, Bern Open Publishing https://doi.org/10.7892/boris.72297
Dilssner F, Springer T, Flohrer C, Dow J (2010) Estimation of phase center corrections for GLONASS-M satellite antennas. J Geod 84(8):467–480. https://doi.org/10.1007/s00190-010-0381-7
Duan B, Hugentobler U, Montenbruck O, Steigenberger P (2023) Performance of Galileo satellite products determined from multi-frequency measurements. J Geod 97(4):32. https://doi.org/10.1007/s00190-023-01723-3
EU (2022) Galileo High Accuracy Service Signal-in-Space Interface Control Document (HAS SIS ICD), European Union, Issue 1.0, May 2022. https://www.gsc-europa.eu/sites/default/files/sites/all/files/Galileo_HAS_SIS_ICD_v1.0.pdf
Fernandez-Hernandez I, Chamorro-Moreno A, Cancela-Diaz S, Calle-Calle JD, Zoccarato P, Blonski D, Senni T, de Blas FJ, Hernández C, Simón J et al (2022) Galileo high accuracy service: initial definition and performance. GPS solutions 26(3):65. https://doi.org/10.1007/s10291-022-01247-x
Ge M, Gendt G, Dick G, Zhang F, Reigber C (2005) Impact of GPS satellite antenna offsets on scale changes in global network solutions. Geophys Res Lett 32(6), https://doi.org/10.1029/2004GL022224
Glaser S, Michalak G, Männel B, König R, Neumayer KH, Schuh H (2020) Reference system origin and scale realization within the future GNSS constellation "Kepler". J Geod 94(12):117. https://doi.org/10.1007/s00190-020-01441-0
GSC (2022) Galileo satellite metadata. http://www.geopp.com/pdf/gpp_cal125_euref19_p.pdf
Haines BJ, Bar-Sever YE, Bertiger WI, Desai SD, Harvey N, Sibois AE, Weiss JP (2015) Realizing a terrestrial reference frame using the Global Positioning System. J Geophys Res: Solid Earth 120(8):5911–5939. https://doi.org/10.1002/2015JB012225
Hauschild A (2017) Basic observation equations. In: Teunissen PJ, Montenbruck O (eds) Springer Handbook of Global Navigation Satellite Systems, Springer, chap 19, pp 561–582, https://doi.org/10.1007/978-3-319-42928-1_19
Huang C, Song S, He L, Chen Q, Jiao W, Zhou W, Jiao G, Zhao H, Yang Y (2023) Estimation of antenna phase center offsets for BDS-3 satellites with the metadata and receiver antenna calibrations. J Geod 97(6):57. https://doi.org/10.1007/s00190-023-01757-7
Huang W, Männel B, Brack A, Schuh H (2021) Two methods to determine scale-independent GPS PCOs and GNSS-based terrestrial scale: comparison and cross-check. GPS Solut 25(1):4. https://doi.org/10.1007/s10291-020-01035-5
Hugentobler U, Montenbruck O (2017) Satellite orbits and attitude. In: Teunissen PJ, Montenbruck O (eds) Springer Handbook of Global Navigation Satellite Systems, Springer, chap 3, pp 59–90, https://doi.org/10.1007/978-3-319-42928-1_3
Johnston G, Riddell A, Hausler G (2017) The International GNSS Service. In: Teunissen P.J., Montenbruck O. (eds), Springer Handbook of Global Navigation Satellite Systems, Springer, chap 33, pp 967–982,https://doi.org/10.1007/978-3-319-42928-1_33
Kersten T, Kröger J, Schön S (2022) Comparison concept and quality metrics for GNSS antenna calibrations. J Geod 96(7):48. https://doi.org/10.1007/s00190-022-01635-8
Kunysz W (2010) Antenna phase center effects and measurements in gnss ranging applications. In: 14th International Symposium on Antenna Technology and Applied Electromagnetics & the American Electromagnetics Conference, IEEE, pp 1–4, https://doi.org/10.1109/ANTEM.2010.5552519
Landskron D, Böhm J (2018) VMF3/GPT3: refined discrete and empirical troposphere mapping functions. J Geod 92(4):349–360. https://doi.org/10.1007/s00190-017-1066-2
Langley RB, Teunissen PJG, Montenbruck O (2017) Introduction to GNSS. In: Teunissen P, Montenbruck O (eds) Springer Handbook of Global Navigation Satellite Systems, Springer, chap 33, pp 967–982, https://doi.org/10.1007/978-3-319-42928-1_1
Liu C, Gao W, Liu T, Wang D, Yao Z, Gao Y, Nie X, Wang W, Li D, Zhang W et al (2020) Design and implementation of a BDS precise point positioning service. Navigation 67(4):875–891. https://doi.org/10.1002/navi.392
Lockheed Martin (2023) GPS-III satellites: Phase center offsets, group delay and inter-signal correction values. https://www.navcen.uscg.gov/gps-technical-references
Lu M, Li W, Yao Z, Cui X (2019) Overview of BDS III new signals. Navigation 66(1):19–35. https://doi.org/10.1002/navi.296
Lyard FH, Allain DJ, Cancet M, Carrère L, Picot N (2021) FES2014 global ocean tides atlas: design and performances. Ocean Sci 17(3):615–649. https://doi.org/10.5194/os-17-615-2021
Mader GL (1999) GPS antenna calibration at the National Geodetic Survey. GPS Solut 3(1):50–58. https://doi.org/10.1007/PL00012780
Maqsood M, Gao S, Montenbruck O (2017) Antennas. In: Teunissen PJ, Montenbruck O (eds) Springer Handbook of Global Navigation Satellite Systems, Springer, chap 17, pp 505–534, https://doi.org/10.1007/978-3-319-42928-1_17
Montenbruck O, Schmid R, Mercier F, Steigenberger P, Noll C, Fatkulin R, Kogure S, Ganeshan AS (2015) GNSS satellite geometry and attitude models. Adv Space Res 56(6):1015–1029. https://doi.org/10.1016/j.asr.2015.06.019
Montenbruck O, Steigenberger P, Villiger A, Rebischung P (2022) On the relation of GNSS phase center offsets and the terrestrial reference frame scale: a semi-analytical analysis. J Geod 96(11):90. https://doi.org/10.1007/s00190-022-01678-x
Montenbruck O, Steigenberger P, Mayer-Gürr T (2024) Manufacturer calibrations of GPS transmit antenna phase patterns: a critical review. J Geod 98(1):2. https://doi.org/10.1007/s00190-023-01809-y
Petit G, Luzum B (2010) IERS conventions (2010). In: IERS Technical Note, vol 36, Verlag des Bundesamts für Kartographie und Geodäsie, Frankfurt am Main, https://www.iers.org/SharedDocs/Publikationen/EN/IERS/Publications/tn/TechnNote36/tn36.pdf
Qu Z, Xu X, Zhao Q, Guo J (2024) Extension of the BDS IGSO and MEO satellite antenna patterns with FengYun-3C and LuTan-1 onboard data. Adv Space Res. https://doi.org/10.1016/j.asr.2024.07.062
Ray JR, Rebischung P, Schmid R (2013) Dependence of IGS products on the ITRF datum. In: Altamimi Z, Collilieux X (eds) Reference Frames for Applications in Geosciences, International Association of Geodesy Symposia, vol 138, Springer, Berlin, Heidelberg, p 63–67, https://doi.org/10.1007/978-3-642-32998-2_11
Rebischung P (2014) Can GNSS contribute to improving the ITRF definition? Phd thesis, Observatoire de Paris
Rebischung P, Schmid R (2016) IGS14/igs14.atx: a new framework for the IGS products. In: AGU Fall Meeting, G41A-0998, San Francisco, US, https://mediatum.ub.tum.de/doc/1341338/file.pdf
Rebischung P, Altamimi Z, Métivier L, Collilieux X, Gobron K, Chanard K (2024) Analysis of the IGS contribution to ITRF2020. J Geod 98(6):49. https://doi.org/10.1007/s00190-024-01870-1
Rodriguez-Solano C, Hugentobler U, Steigenberger P, Lutz S (2012) Impact of earth radiation pressure on GPS position estimates. J Geod 86(5):309–317. https://doi.org/10.1007/s00190-011-0517-4
Schmid R, Rothacher M (2003) Estimation of elevation-dependent satellite antenna phase center variations of GPS satellites. J Geod 77(7–8):440–446. https://doi.org/10.1007/s00190-003-0339-0

Schmid R, Rothacher M, Thaller D, Steigenberger P (2005) Absolute phase center corrections of satellite and receiver antennas: Impact on global GPS solutions and estimation of azimuthal phase center variations of the satellite antenna. GPS Solut 9(4):283–293. https://doi.org/10.1007/s10291-005-0134-x

Schmid R, Steigenberger P, Gendt G, Ge M, Rothacher M (2007) Generation of a consistent absolute phase-center correction model for GPS receiver and satellite antennas. J Geod 81(12):781–798. https://doi.org/10.1007/s00190-007-0148-y

Schmid R, Dach R, Collilieux X, Jäggi A, Schmitz M, Dilssner F (2016) Absolute IGS antenna phase center model igs08. atx: status and potential improvements. J Geod 90(4):343–364, https://doi.org/10.1007/s00190-015-0876-3

Seitz M, Blossfeld M, Glomsda M, Angermann D, Rudenko S, Zeitlhoefler J, Seitz F (2023a) DTRF2020: Strategy, Results and Data Set. In: EGU General Assembly Conference Abstracts, EGU–12029, https://doi.org/10.5194/egusphere-egu23-12029

Seitz M, Blossfeld M, Glomsda M, Rudenko S, Zeitlhoefler J, Seitz F (2023) DTRF2020. Zenodoo. https://doi.org/10.5281/zenodo.8369167

Springer TA (2000) Modeling and validating orbits and clocks using the Global Positioning System, Geodätisch-geophysikalische Arbeiten in der Schweiz, vol 60. Schweizerische Geodätische Kommission

Steigenberger P, Montenbruck O (2023) Consistency of Galileo satellite antenna phase center offsets. J Geod 97(6):58. https://doi.org/10.1007/s00190-023-01750-0

Steigenberger P, Fritsche M, Dach R, Schmid R, Montenbruck O, Uhlemann M, Prange L (2016) Estimation of satellite antenna phase center offsets for Galileo. J Geod 90(8):773–785. https://doi.org/10.1007/s00190-016-0909-6

Steigenberger P, Thoelert S, Montenbruck O (2018) GNSS satellite transmit power and its impact on orbit determination. J Geod 92(6):609–624. https://doi.org/10.1007/s00190-017-1082-2

Steigenberger P, Thoelert S, Dach R, Montenbruck O (2024) Validation of GPS III transmit antenna calibrations. Adv Space Res 73(5):2488–2498. https://doi.org/10.1016/j.asr.2023.11.048

Strasser S, Mayer-Gürr T, Zehentner N (2019) Processing of GNSS constellations and ground station networks using the raw observation approach. J Geod 93(7):1045–1057. https://doi.org/10.1007/s00190-018-1223-2

Villiger A (2019) [IGSMAIL-7733] igs14_2038: Update including updated PCO/PV for GPS III satellite G074. https://lists.igs.org/pipermail/igsmail/2019/007729.html

Villiger A (2022) [IGS-ACS-1570] Update igs20_2221.atx including BLOCK IIIA x/y-pco update and BEIDOU, QZSS and IRNSS

Villiger A, Dach R, Schaer S, Prange L, Zimmermann F, Kuhlmann H, Wübbena G, Schmitz M, Beutler G, Jäggi A (2020) GNSS scale determination using calibrated receiver and Galileo satellite antenna patterns. J Geod 94(9):93. https://doi.org/10.1007/s00190-020-01417-0

Villiger A, Dach R, Prange L, Jäggi A (2021) Extension of the repro3 ANTEX file with BeiDou and QZSS satellite antenna pattern. In: EGU General Assembly 2021, Online, 19-30 April, https://doi.org/10.5194/egusphere-egu21-6287

Wu JT, Wu SC, Hajj G, Bertiger W, Lichten SM (1993) Effects of antenna orientation on GPS carrier phase. Manuscr Geod 18:91–98

Wübbena G, Schmitz M, Warneke A (2019) Geo++ absolute multi-frequency GNSS antenna calibration. In: EUREF Analysis Center (AC) Workshop, Warsaw, Poland, http://www.geopp.com/pdf/gpp_cal125_euref19_p.pdf

Xia F, Ye S, Chen D, Wu J, Wang C, Sun W (2020) Estimation of antenna phase center offsets for BeiDou IGSO and MEO satellites. GPS Solut 24(4):90. https://doi.org/10.1007/s10291-020-01002-0

Yang Y, Xu Y, Li J, Yang C (2018) Progress and performance evaluation of BeiDou global navigation satellite system: Data analysis based on BDS-3 demonstration system. Science China Earth Sciences 61(5):614–624. https://doi.org/10.1007/s11430-017-9186-9

Yuan Y, Li X, Yao Y, Huang S, Wang Q, Zhang K (2024) Estimation of phase center corrections for BDS satellites aligned to the IGS20 frame. GPS Solut 28(2):63. https://doi.org/10.1007/s10291-023-01603-5

Zajdel R, Steigenberger P, Montenbruck O (2022) On the potential contribution of BeiDou-3 to the realization of the terrestrial reference frame scale. GPS Solut 26(4):109. https://doi.org/10.1007/s10291-022-01298-0

Zehentner N (2016) Kinematic orbit positioning applying the raw observation approach to observe time variable gravity. PhD thesis, Graz University of Technology

Zeimetz P, Kuhlmann H (2008) On the accuracy of absolute GNSS antenna calibration and the conception of a new anechoic chamber. In: Proceedings of the FIG Working Week, Stockholm, Sweden,

Zhao Q, Guo J, Wang C, Lyu Y, Xu X, Yang C, Li J (2022) Precise orbit determination for BDS satellites. Satell Nav 3(1):2. https://doi.org/10.1186/s43020-021-00062-y

Zhu S, Massmann FH, Yu Y, Reigber C (2003) Satellite antenna phase center offsets and scale errors in GPS solutions. J Geod 76(11–12):668–672. https://doi.org/10.1007/s00190-002-0294-1